Local production, downward and regional transport aggravated surface ozone pollution during the historical orange-alert large-scale ozone episode in eastern China

Yibo Zhang, Shaocai Yu, Xue Chen, Zhen Li, Mengying Li, Zhe Song, Weiping Liu, Pengfei Li, Xiaoye Zhang, Eric Lichtfouse, et al.

Local production, downward and regional transport aggravated surface ozone pollution during the historical orange-alert large-scale ozone episode in eastern China

Yibo Zhang[1] · Shaocai Yu[1,2] · Xue Chen[1] · Zhen Li[1] · Mengying Li[1] · Zhe Song[1] · Weiping Liu[1] · Pengfei Li[3] · Xiaoye Zhang[1,4] · Eric Lichtfouse[5] · Daniel Rosenfeld[6]

Abstract

Increasing severe and persistent ozone pollution in China has resulted in serious harm to human health in recent years, yet the precise pollution sources are poorly known because there is few knowledge on large-scale extreme ozone episodes. Here, we studied the formation of the historical orange-alert regional ozone episode in eastern China on 6 June, 2021, by combining process analysis, integrated source apportionment modelling, and chemical and meteorological data. Results show that dur-ing the pollution episode, 94% of cities in eastern China suffered ozone pollution, and 39% had daily maximum 8-h average ozone concentrations higher than 100 ppb. This is explained by favorable local ozone formation and transports provided by the prevailing northwestern winds in the upper air, and by sinking atmospheric motions favoring the persistence of high surface ozone concentrations. During daytime, local photochemical production induced an ozone increase of 0.3–28.4 ppb h^{-1} and vertical transport induced an ozone increase of 0.4–56.1 ppb h^{-1}. As a consequence, vertical downward transport of ozone generated in the upper air by photochemical reactions aggravated surface ozone pollution. Surface ozone concentrations include 25.8–53.9% of ozone from local provincial emissions, 0–42.6% of ozone from inter-regional transports from neigh-boring regions, 4.6–23.1% of ozone from outer-regional transport, and 13.6–52.9% of ozone from boundary conditions in the selected cities. Overall, our findings show that favorable meteorological conditions promoted the chemical productions of ozone on the surface and at high altitudes, thus resulting in this heavy ozone pollution. In addition, regional and vertical downward transports of aloft ozone further aggravated the surface ozone pollution, leading to the large-scale extreme ozone pollution episode.

Keywords Ozone pollution · Meteorological conditions · Process analysis · Photochemical production · Vertical transport · Source contributions

✉ Shaocai Yu
shaocaiyu@zju.edu.cn

✉ Pengfei Li
lpf_zju@163.com

Eric Lichtfouse
eric.lichtfouse@gmail.com
https://cv.archives-ouvertes.fr/eric-lichtfouse

[1] Key Laboratory of Environmental Remediation and Ecological Health, Ministry of Education; Research Center for Air Pollution and Health, College of Environmental and Resource Sciences, Zhejiang University, Hangzhou, Zhejiang 310058, People's Republic of China

[2] Division of Chemistry and Chemical Engineering, California Institute of Technology, Pasadena, CA 91125, USA

[3] College of Science and Technology, Hebei Agricultural University, Baoding 071000, Hebei, People's Republic of China

[4] China Meteorological Administration, Chinese Academy of Meteorological Sciences, Beijing 100081, People's Republic of China

[5] Aix-Marseille Univ, CNRS, Coll France, CNRS, INRA, IRD, CEREGE, Avenue Louis Philibert, 13100 Aix en Provence, France

[6] Institute of Earth Sciences, Hebrew University of Jerusalem, Jerusalem, Israel

Introduction

Tropospheric ozone (O_3) is a primary air pollutant and an important greenhouse gas, which affects the Earth's radiative forcing, and endangers terrestrial vegetation and human health (Skarby et al. 1998; Jerrett et al. 2009; Lelieveld et al. 2015). In recent years, China has experienced high ozone levels in air due to intensive anthropogenic emissions from the rapid urbanization and industrialization (Cheng et al. 2018; Nie et al. 2019; Sun et al. 2019; Li et al. 2020). Ozone pollution has become a severe air quality issue in China, particularly in the summer of major city clusters such as the North China Plain, the Yangtze River Delta, the Sichuan Basin, and the Fenwei Plain (Verstraeten et al. 2015; Li et al. 2017; Wang et al. 2017; Lu et al. 2018, 2020). Compared to the developed regions abroad, in China the daily maximum 8-h average ozone (MDA8 O_3) concentrations in the warm season are 6.3–16% higher (Lu et al. 2018). In the summer of 2013–2017, the maximum values of MDA8 O_3 in the North China Plain reached 150 ppb (Li et al. 2019; Lu et al. 2020). From 2013 to 2019, the MDA8 O_3 concentrations in the warm seasons at Chinese sites increased at a rate of 2.4 ppb per year, and about 30% of monitoring sites showed an increase of more than 3.0 ppb per year. The MDA8 ozone concentration in the Yangtze River Delta increased by 1.8 ppb per year in the warm season from 2014 to 2018. The rise in ozone levels was also witnessed in Europe, the United States, India and Korea (Jenkin. 2008; Paoletti et al. 2014; Guo et al. 2018, Finch and Palmer 2020, Vellingirl et al. 2016, Gao et al., 2020, 2021).

Measures of emission controls in Europe and America induced a decrease of ozone maxima and magnitudes (Paoletti et al. 2014; Simon et al. 2015; Chang et al. 2017; Lu et al. 2018; Finch and Palmer 2020). Whereas in China ozone levels increased substantially despite air cleaning action plans launched by the government. This is partly due to the unexpected fact that decreasing ozone precursors may worsen ozone pollution (Wang et al. 2020, 2021). For instance, sharp declines of particulate matter content ($PM_{2.5}$) were partly responsible for the ozone increases in the North China Plain, because HO_2 radicals were less neutralized by aerosol particles and, in turn, stimulated ozone productions (Li et al. 2019). A similar effect was observed for NO_x in China, the reductions of NO_x emissions in 2013–2019 were associated with an increase of daily ozone in March, and with a longer duration of the ozone pollution season, extending from summer to winter-spring.

Intensive researches have focused on the characteristics, factors and mechanisms of ozone pollution episodes. Meteorological conditions control ozone formation and fate by influencing photochemical reactions, advection, convection and dry deposition (Jacob and Winner 2009; Pu et al. 2017; Han et al. 2018; Li et al. 2020). For instance, in summer the large-scale anticyclone and foehn wind induce a hot and dry weather, causing extreme heat waves and serious ozone pollution in the North China Plain (Chen and Lu 2016; Gong and Liao 2019; Li et al. 2020). High ozone episodes in many countries show similar characteristics closely related to active photochemical formations, heat wave, prevailing wind conditions, anticyclone synoptic systems, tropospheric intrusions, and regional transports of air masses containing ozone-rich air from upwind areas (Jin et al. 2008; Gao et al. 2016; Schnell et al. 2016, Kalabokas et a. 2017; Pu et al. 2017, Shu et al. 2019; Gong et al. 2020; Jaen et al. 2021; Yang et al. 2021). Ozone pollution episodes in eastern China have been intensively investigated (Gao et al. 2016; Li et al. 2017; Shu et al. 2019; Gong et al. 2020; Mao et al. 2020). The sinking motions and temperature inversions were proposed to cause ozone pollution in the Beijing-Tianjin-Hebei area (Mao et al. 2020)**.** To gain further insight on mechanisms of ozone transports and accumulations, we studied here the large-scale ozone pollution that occurred in eastern China on June 6, 2021, lasting 4 days and causing more than 0.3 billion people to be exposed.

Experimental

Data sources

Provinces and province-level municipalities in eastern China with high ozone concentrations, including Beijing, Tianjin, Hebei, Henan, Shaanxi, Shanxi, Shandong, Anhui and Jiangsu, were selected to investigate this heavy ozone pollution episode (Figs S1a,b). The hourly concentrations of ozone and NO_2 during the study period were obtained from the China Ministry of Ecology and Environment (beijingair.sinaapp.com). A total of 591 monitoring sites were collected from 95 cities in eastern China to analyze the characteristics of the ozone pollution. According to the "Ambient Air Quality Standard" in China (MEP, 2012), the air quality levels were divided into five categories based on the monitored maximum daily 8-h average ozone (MDA8 O_3) concentrations: excellent (green, 0–47 ppb), good (yellow, 47–75 ppb), lightly polluted (orange, 75–100 ppb), moderately polluted (red, 101–123 ppb), and heavily polluted (purple, 124–374 ppb) in the current study.

Model configuration

We simulated the high ozone pollution episode in eastern China from 5 to 10 June 2021 using the Weather Research and Forecasting-Community Multiscale Air Quality (WRF-CMAQ) modeling system. We focused on the formation of severe ozone pollution on 6 June, 2021, which was the most serious ozone pollution day after the launch of the ozone orange alert. The WRF/CMAQ model was configured at a horizontal resolution of 12 km × 12 km and 29 vertical levels, covering the central-eastern China and surrounding Korea (Fig S1). The detailed model configuration is the same as Yu et al. (2014) and is briefly described in Supplementary Material. The first seven days of model simulations were taken as the spin-up period to minimize the effects of initial chemical conditions.

The ozone formation within each time step contributed by gas-phase chemistry (CHEM), vertical turbulent diffusion (VDIF), horizontal diffusion (HDIF), vertical advection (ZADV), horizontal advection (HADV), cloud chemistry (CLDS), and dry deposition (DDEP) were calculated using the Integrated Process Rate (IPR) analysis method embedded in the CMAQ model. In our study, HTRA (HADV + HDIF) and VTRA (ZADV + VDIF) were used to represent the net effects of horizontal and vertical transports on the ozone formation, respectively.

The source contributions of ozone concentrations were evaluated by the CMAQ model combined with ISAM (Kwok et al. 2015). Based on geographical distributions and the spatial characteristics of ozone pollution, 12 regions including Shaanxi, Shanxi, Beijing-Tianjin-Hebei, Shandong, Henan, Hebei, Jiangxi, Anhui, Jiangsu, Shanghai, Zhejiang and other region (OTH) inside eastern China were set as tracked source regions of ozone concentrations using the ISAM source apportionment method (supplementary Fig S1a). Statistical measures including the mean bias (MB), the normalized mean bias (NMB), and the correlation coefficient (R) were used to evaluate the model performances (Yu et al. 2006; 2014). The evaluation results were presented in Supplementary Material.

Results and discussion

Characteristics of ozone pollution and diurnal patterns

We studied the large-scale ozone pollution that occurred in eastern China on June 6, 2021, and lasted for 4 days. The spatial distributions of the MDA8 O_3 concentrations and the duration hours of ozone pollution on 6 June, 2021 are shown in Figs. 1 a,b. Ozone pollution refers to hourly ozone concentrations exceeding the threshold of 74.8 ppb (160 μg m^{-3}) in China. The Beijing-Tianjin-Hebei and Yangtze River Delta regions, and Shandong and Henan provinces displayed slight ozone pollution on 5 June, 2021 (Fig. S2). On June 6, with the rapid increase of ozone concentrations, a large-scale ozone pollution occurred in eastern China. Most cities experienced severe ozone pollution, for instance in 11 of the 12 cities in Beijing-Tianjin-Hebei, 16 of the 17 cities in Henan, 14 of the 16 cities in Anhui, 9 of the 11 cities in Shanxi, and 10 of the 10 cities in Shaanxi. Such a large-scale regional ozone pollution in 89 out of 95 cities (93.7%) in eastern China has seldom been witnessed in China, Europe and the United States (Paoletti et al. 2014; Xue et al. 2014; Lu et al. 2018; Liu et al. 2020).

The MDA8 O_3 concentrations in Beijing-Tianjin-Hebei, Henan, Anhui Shanxi and Shaanxi provinces ranged from 46.1 to 133.1 ppb. All cities in Shandong and Jiangsu provinces had heavy ozone pollution with average MDA8 O_3 concentrations of 103.3 and 100.8 ppb, respectively. Several cities in Henan and Anhui displayed severer ozone pollution as well. For example, the MDA8 O_3 concentrations in Zhengzhou and Xian reached 134.6 and 135.6 ppb, respectively, far exceeding the 74.8 ppb threshold.

Overall, the ozone pollution in eastern China on June 6, 2021, was much more serious than previous reports. Here, we focused on June 6, 2021, during which ozone pollution was the most serious. We selected 7 major cities, namely Xi'an, Linfen, Hengshui, Zhengzhou, Dezhou, Huainan and Suzhou to investigate the diurnal variations of ozone pollution. These seven cities were chosen because of their most serious ozone pollution levels among the seven target regions in eastern China. Another city, Taian in Shandong province, was also selected for comparison (Fig. S1b).

The simulated and observed concentrations of ozone and NO_2 in Zhengzhou, Suzhou, Xi'an and Dezhou on 6 June, 2021 are exhibited in Figs. 1 c,d. Results show that eight cities displayed very high ozone concentrations exceeding the grade II national standard of 93.5 ppb (200 μg m^{-3}), and long exceedance duration from 11:00 to 20:00. On june 6, ozone concentrations decreased from midnight and reached the lowest value at about 6:00 in the morning due to the alleviating effects of NOx titration. Then ozone concentrations began to increase at 7:00. Compared with other studies, ozone concentrations in Zhengzhou, Suzhou and other five selected cities exhibited broader peak duration patterns from 14:00 to 18:00. This pattern could be driven by chemical productions, transports, and precursor emissions (Zhang et al. 2004; Xia et al. 2021; Xu et al. 2021). NO_2 showed opposite diurnal variations versus ozone with the peak at 6:00–8:00 in the morning due to the combined effects of night accumulation and morning traffic emissions. Overall, we found that ozone pollution lasted for a longer time and had broader peak patterns than previous reports.

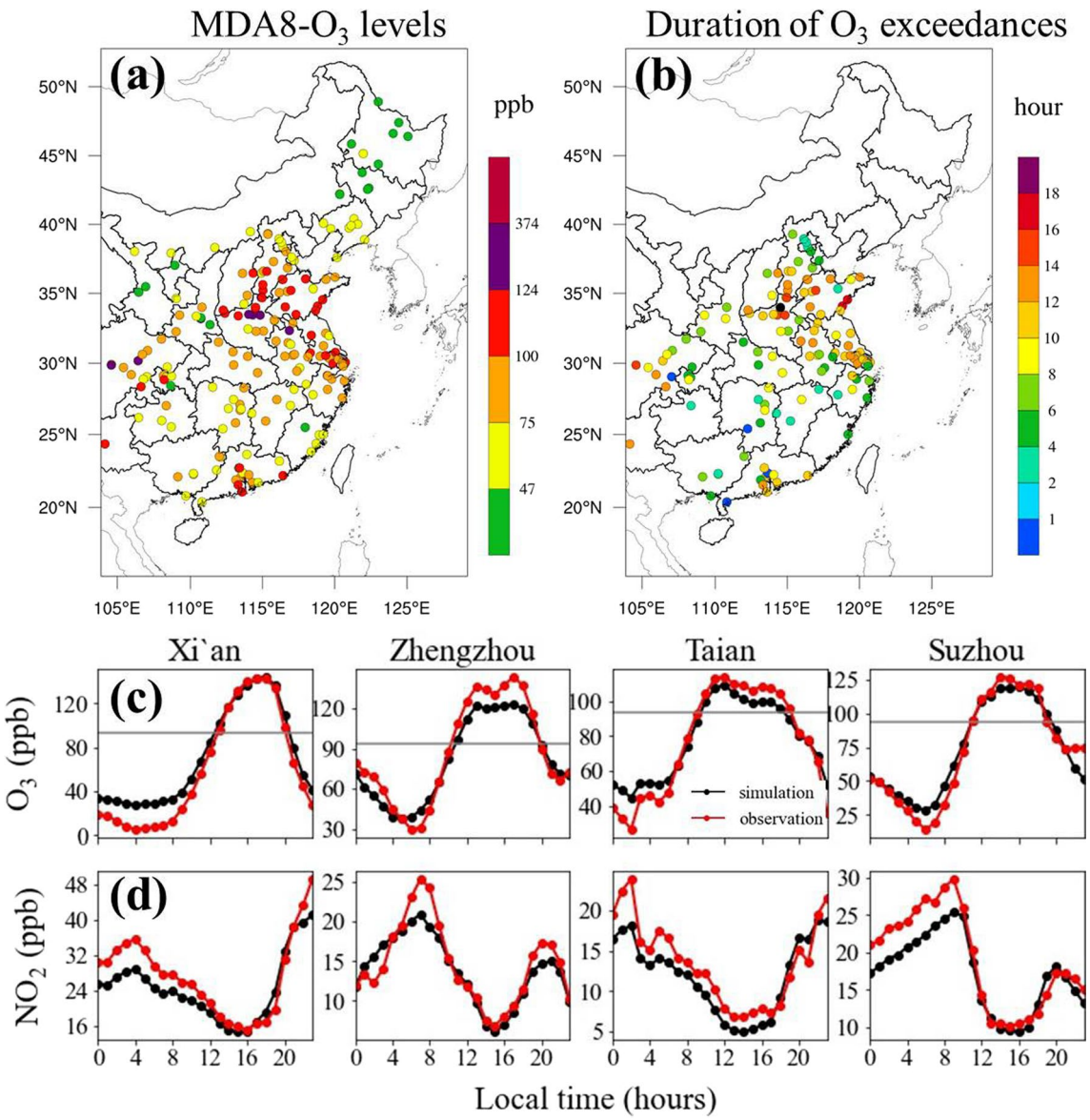

Fig. 1 Spatial distributions of observed a) daily maximum 8-h average ozone concentrations (MDA8); b) number of hours with ozone concentrations exceeding 74.8 ppb in the monitoring stations over eastern China on June 6, 2021. Diurnal variations of observed versus simulated c) ozone concentrations and d) NO_2 concentrations in four typical cities (Xi'an, Zhengzhou, Taian and Suzhou) on June 6, 2021. The grey lines in c) represent the grade II of national ozone standard of 93.5 ppb. Results show that the ozone pollution in eastern China on June 6, 2021, was very serious with high ozone concentrations and long durations of ozone exceedances

Spatio-temporal evolutions of ozone pollution and meteorological conditions

The meteorological conditions on June 6, 2021 are depicted in Fig S4 and described in supplementary text. Spatio-temporal evolutions of simulated and observed ozone concentrations and corresponding meteorological fields at 8:00, 12:00, 16:00, and 20:00 on 6 June, 2021 are shown in Figs. 2 a–c. From 8:00 to 12:00, the surface temperature rose significantly and relative humidity decreased rapidly because of the rise of solar radiation. Indeed, solar radiation reaching the ground directly induces the continuous increases of temperature and the decreases of relative humidity (Boer, 1993). We observed that ozone concentrations in Henan, Shandong, Anhui and Jiangsu provinces increased promptly due to favorable meteorological conditions with temperature higher than 32℃ and relative humidity lower than 50%. This enhanced ozone formation resulted in ozone concentrations exceeding the standard of 93.5 ppb in multiple cities. High temperatures are generally considered to be a good predictor of high ozone levels because temperature favors ozone production by influencing chemical reactions and emission

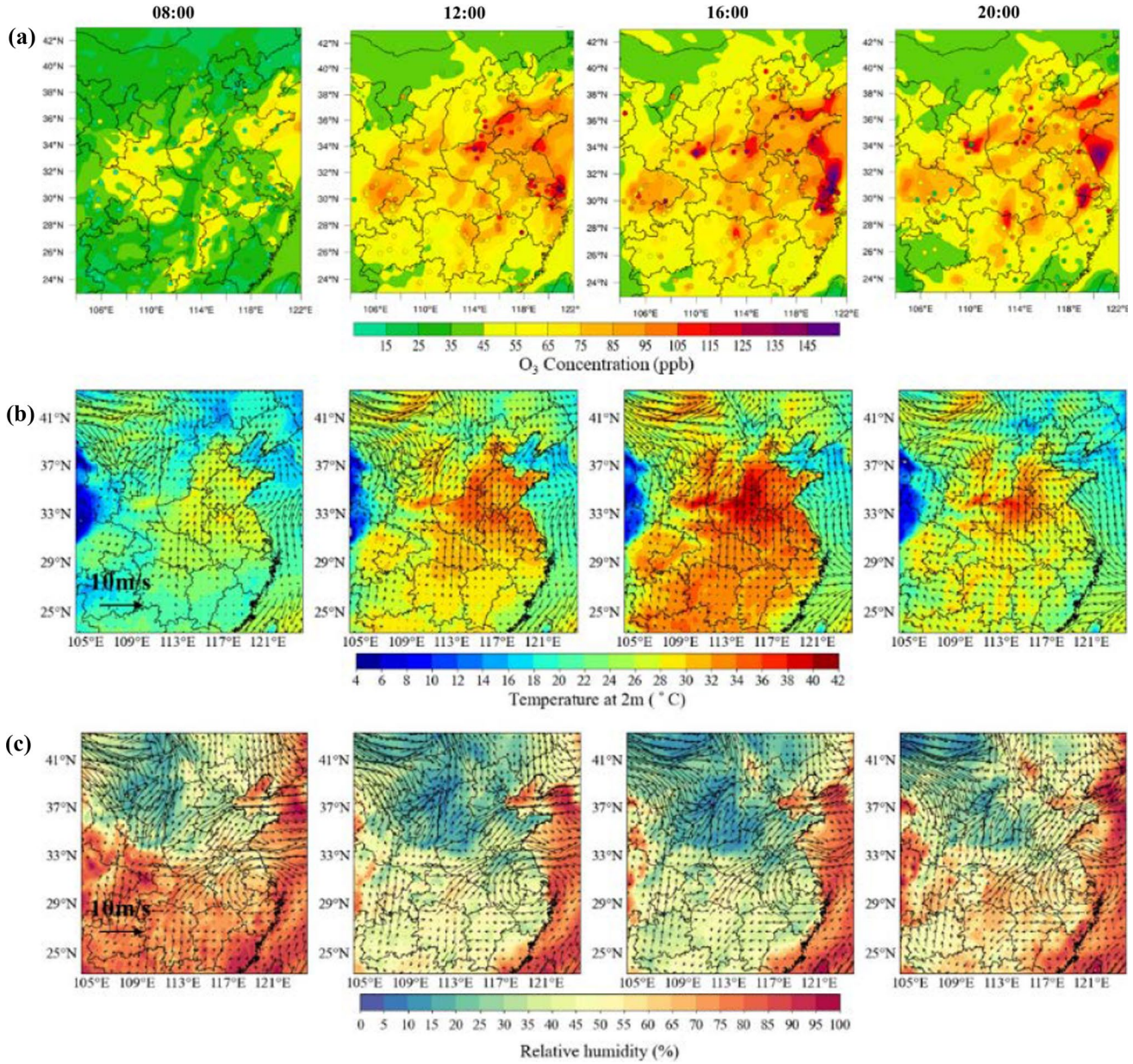

Fig. 2 Temporal evolutions for (**a**) overlaies of simulated (color contour) and observed (colored circles) ozone concentrations; **b** 10 m wind and 2 m temperature fields; **c** wind field at 850 hPa and surface relative humidity fields over eastern China at 8:00, 12:00, 16:00, and 20:00 (UTC time) on 6 June, 2021. UTC: coordinated universal time. Both the simulated and observed data show that the under favorable meteorological conditions with high temperature, low relative humidity and anticyclone, ozone concentrations increased rapidly within several hours, resulting in the large-scale ozone pollution in eastern China

rates (Jacob and Winner, 2009; Bloomer et al. 2009). Similarly, for temperatures above 30℃ during 2010–2017, the mean summer ozone levels increased by 6.65 and 13.68 ppb per degree in urban and remote sites, respectively (Gu et al. 2020).

From 12:00 to 16:00, the elevated and persistent high temperatures aggravated ozone pollution and caused the simulated ozone pollution to spread further into the whole studied region, in agreement with the observed data (Fig. 2a). The hourly ozone peak concentrations reached over 145 ppb in Xi'an, Zhengzhou and Suzhou. The highest temperatures of over 40℃ were observed at the junction of Beijing-Tianjin-Hebei, Henan and Shandong, being also the places with the most serious ozone pollution. This is partly explained by a low-pressure system (Fig. S4b), which was known for weak diffusion of ozone and precursors and, in turn, accumulation of pollutants (Otero et al. 2016; Liu et al. 2019; Yang et al. 2021).

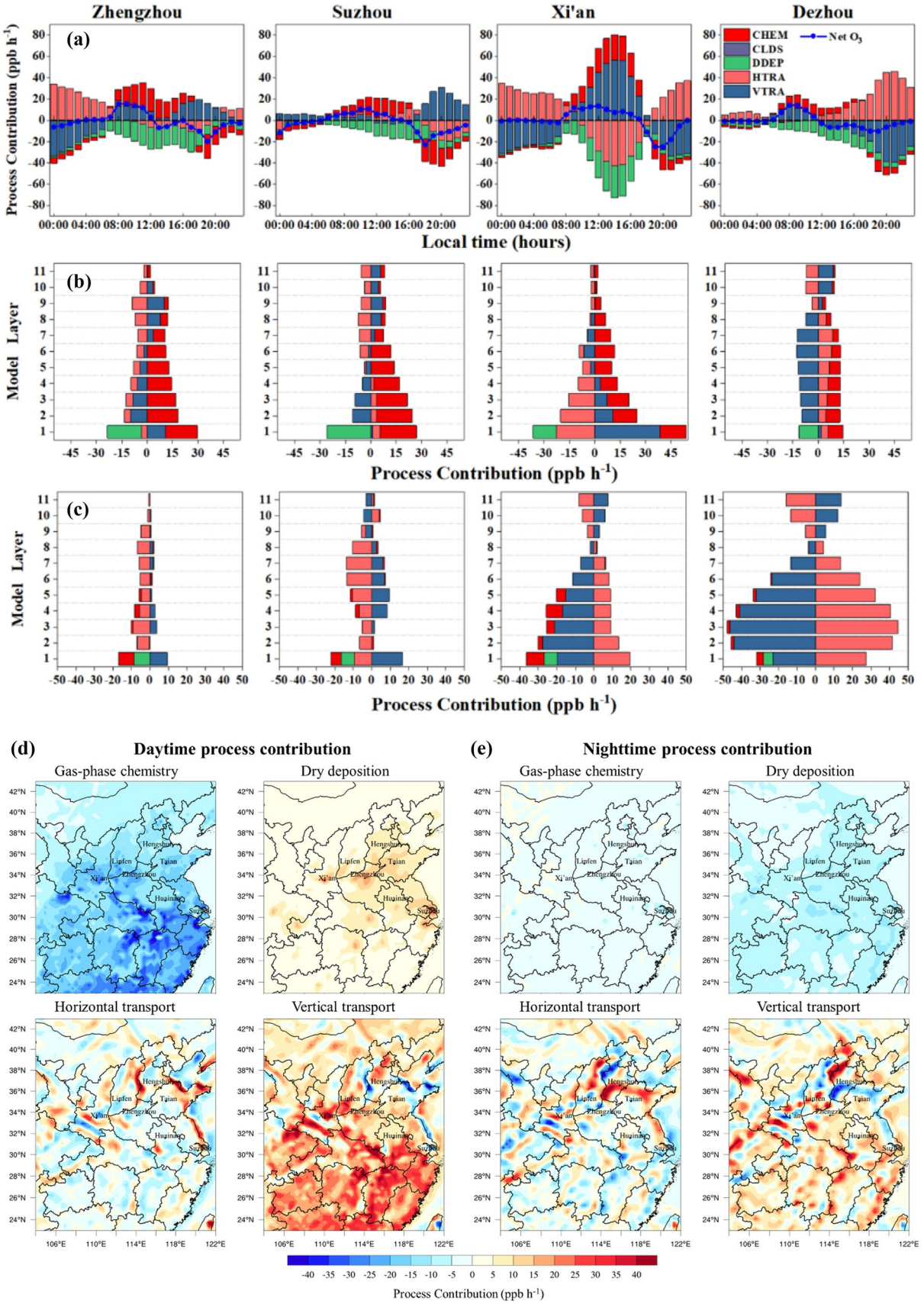
Zhengzhou
Suzhou
Xi'an
Dezhou
(a)
Process Contribution (ppb h-1)
CHEM
CLDS
DDEP
HTRA
VTRA
Net O3
Local time (hours)
(b)
Model Layer
Process Contribution (ppb h-1)
(c)
Model Layer
Process Contribution (ppb h-1)
(d)
Daytime process contribution
(e)
Nighttime process contribution
Gas-phase chemistry
Dry deposition
Horizontal transport
Vertical transport
Hengshui
Lipfen
Taian
Xi'an
Zhengzhou
Huaimao
Suzhou
Process Contribution (ppb h-1)

◂**Fig. 3** **a** Hourly contributions of gas-phase chemistry (CHEM), cloud chemistry (CLDS) dry deposition (DDEP), horizontal transport (HTRA) and vertical transport (VTRA) to ozone formation, with blue line presenting the net ozone changes. **b** Vertical profiles of daytime (8:00–16:00) and **c** nighttime (17:00–23:00) mean process contributions to ozone changes at different heights. **d** daytime and **e** nighttime average contributions of gas chemistry, dry deposition, horizontal transport, and vertical transport to ozone formation on 6 June of 2021 in eastern China. Results show that gas-phase chemistry and vertical transport processes highly increased the level of surface ozone concentrations during daytimes.

Horizontal transports of ozone from the surrounding areas also contributed to the observed ozone rises. Indeed, air masses rich in ozone and ozone precursors from the heavily polluted Henan province were transported to Shandong, worsening the air quality in Shandong. Air masses from Inner Mongolia brought dry air to Shaanxi, making relative humidity lower than 20%, which promoted the local photochemical formations of ozone. Regional transports of NOx and volatile organic compounds (VOCs) from the surrounding areas contributed to the high ozone concentrations in Shanxi (Fig S5).

Controlled by the anticyclone, the sinking motions in the Yangtze River Delta constrained the diffusion of ozone within the lower atmosphere. The surface ozone pollution was further enhanced by the downward transport of high-altitude ozone in the Yangtze River Delta (Fig. 1b). After the sunset, the decrease of temperature, the cessation of ozone photochemical formation, the NOx titration effect, and the increase of relative humidity all accelerated ozone decomposition, resulting in the rapid decline of ozone levels. Nonetheless, at 20:00, ozone concentrations at the junction of Beijing-Tianjin-Hebei, Henan and Shandong provinces were still high, which was explained by ozone transport from the sea. The model overestimated ozone concentrations in regions with low ozone values, but still captured the spatial distributions of ozone in eastern China. Generally, the model well reproduced the evolution processes of ozone pollution on 6 June, 2021. The spatio-temporal evolutions of ozone pollution and corresponding meteorological conditions from 5 to 10 June, 2021 are presented in Fig S6 and discussed in Supplementary Material. Overall, we analyzed the spatio-temporal evolution processes of ozone pollution on 6 June, 2021, using model simulations and monitoring data. We found that the meteorological conditions on June 6 induced the rapid growth and the rapid expansion of regional ozone pollution.

Mechanisms of ozone formation and transport

We quantified the contributions of the following processes to ozone pollution during the severe ozone pollution episode in eastern China: 1) gas-phase chemistry, 2) horizontal advection and diffusion, 3) vertical advection and diffusion, 4) cloud chemistry, and 5) dry deposition. The hourly contributions of each process to modelling surface ozone concentration changes in Zhengzhou, Suzhou, Xi'an and Dezhou on 6 June, 2021, are shown in Fig. 3a. The net ozone concentration changes were mainly caused by gas chemistry, horizontal transport, vertical transport, and dry deposition, while cloud chemistry had negligible contributions due to the absence of clouds. This is consistent with other studies in the Pearl River Delta and Yangtze River Delta (Wang et al. 2010, Shu et al. 2016). For surface ozone, dry deposition was the primary sinking process, while gas-phase chemistry was the major process during daytime (8:00–16:00) and the consumption process during the remaining hours. Horizontal and vertical transports either increased or decreased surface ozone concentrations of the target cities, depending mainly on local atmospheric circulations. For example, after 16:00, vertical transport contributed to the ozone increase in Zhengzhou and Suzhou, but decreased ozone in Xi'an and Dezhou. The ozone levels in Xi'an during 9:00–18:00 were significantly enhanced by vertical transports (4.5–61.6 ppb h^{-1}). However, the enhancement effects of vertical transports on ozone levels were offset by the combined effects of horizontal transports and dry deposition. In general, the effects of horizontal transports on ozone formation were opposite to those of vertical transports.

The average contributions over daytime for gas-phase chemistry, dry deposition, vertical transport and horizontal transport to ozone concentration changes in Zhengzhou, Suzhou, Xi'an and Dezhou at different heights are presented in Fig. 3b. Dry deposition, as the most important ozone sink on the ground, consumed daytime ozone at -20.0 ppb/h in Zhengzhou, -13.7 ppb/h in Suzhou, -22.0 ppb/h in Xi'an, and -11.3 ppb/h in Dezhou. Gas-phase chemistry contributed positively to daytime ozone rises at both near-surface and aloft levels (from 125 to 2500 m above ground, model layers 2–11), with the average contributions of 1.1–18.8 ppb/h in Zhengzhou, 1.0–15.4 ppb/h in Suzhou, 1.3–21.5 ppb/h in Xi'an, and 1.3–8.8 ppb/h in Dezhou.

Our results show that the photochemistry in the surface layer of Suzhou was stronger than those at high altitudes. This contrasts with the results of Li et al. (2012) who found that the photochemical reactions at the height of 300–1500 m were stronger than those at ground level during August in the Yangtze River Delta. The daytime mean contributions of vertical transport to the surface ozone were 10.8 ppb/h in Zhengzhou and 33.8 ppb/h in Xi'an. For Suzhou, vertical transport showed little contribution to surface ozone with 0.9 ppb/h, but vertical downward transport increased aloft ozone at 1.4–10.8 ppb/h. The negative contributions of vertical transport to ozone in the upper air confirmed the positive contribution of vertical downward transports to near-surface ozone pollution (Figs. 3b and S7b), in agreement with Gao

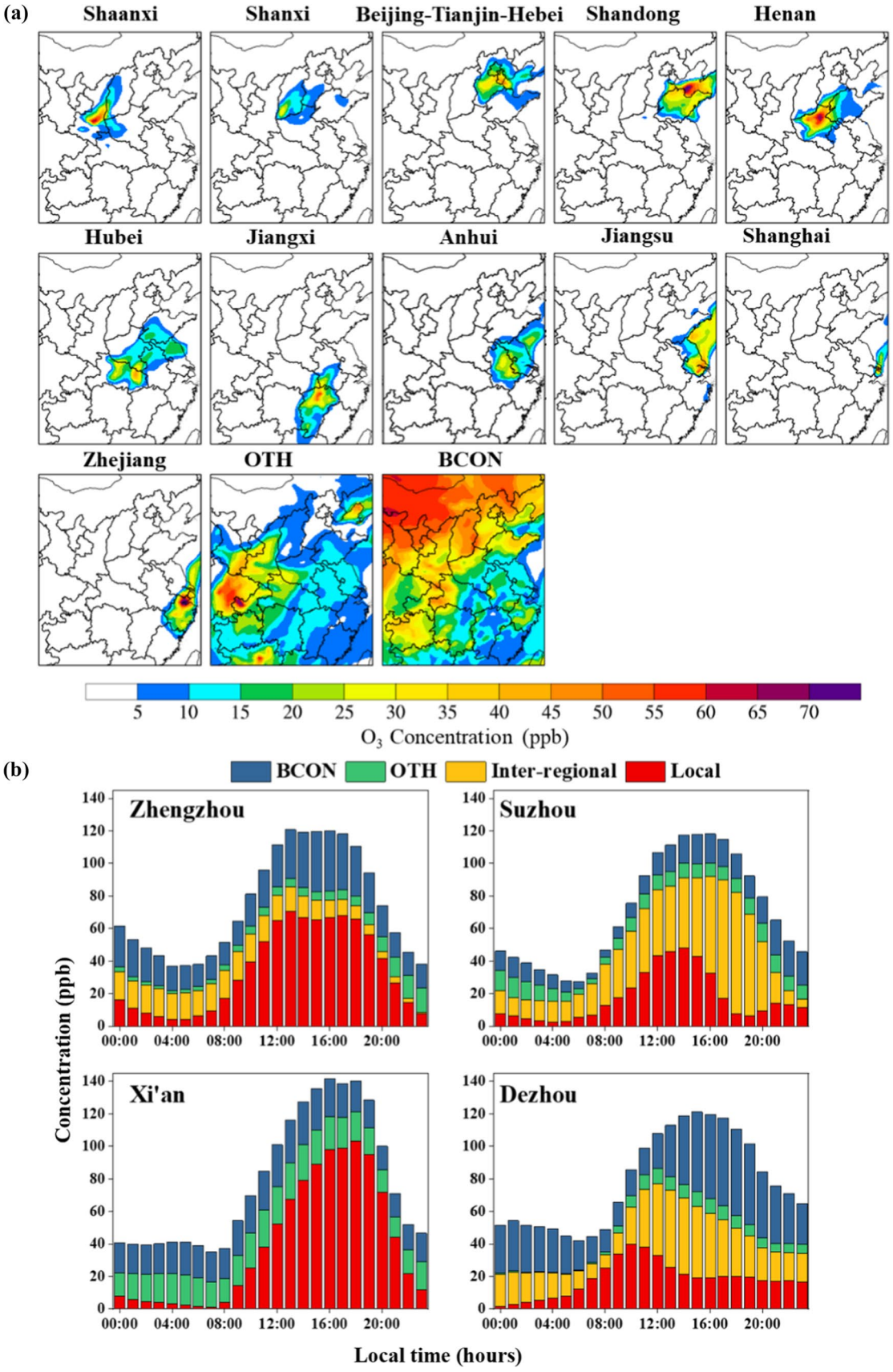
(a)
Shaanxi
Shanxi
Beijing-Tianjin-Hebei
Shandong
Henan
Hubei
Jiangxi
Anhui
Jiangsu
Shanghai
Zhejiang
OTH
BCON
5 10 15 20 25 30 35 40 45 50 55 60 65 70
O3 Concentration (ppb)
(b)
BCON
OTH
Inter-regional
Local
Zhengzhou
Suzhou
Xi'an
Dezhou
Concentration (ppb)
00:00 04:00 08:00 12:00 16:00 20:00
Local time (hours)

◂**Fig. 4** **a** Spatial distributions of simulated daytime (8:00–16:00) ozone concentrations from each source region; **b** time-series of ozone source apportionments of ozone in Zhengzhou, Suzhou, Xi'an and Dezhou contributed by local provincial-level (Local), interregional, OTH (other areas in the simulation domain except the Beijing-Tianjin-Hebei, Shanxi, Shaanxi, Shandong, Henan, Hubei, Jiangxi, Anhui, Jiangsu, Shanghai and Zhejiang) and boundary conditions (BCON) on 6 June, 2021. Results show that local emissions and regional transport from surrounding regions have important contributions to the ozone pollution in eastern China on 6 June, 2021.

et al. (2016) and Shu et al. (2019). Horizontal transport decreased ozone in Zhengzhou, Xi′an and Linfen because their ozone was transported to their downwind areas.

The daytime and nighttime mean contributions of gas-phase chemistry, horizontal transport, vertical transport and dry deposition to ozone formation at the model-surface level in eastern China on 6 June, 2021 are displayed in Figs. 3d and e. Gas-phase chemistry and vertical transport were the main contributors to daytime ozone increases in eastern China, with positive contributions of 0.3–28.4 and 0.4–56.1 ppb h^{-1}, respectively. Simular to the previous studies (Shu et al. 2016; Zheng et al. 2021; Tang et al. 2021), different processes affect the formation and consumption of ozone in eastern China. Overall, we found that the high concentrations of surface ozone in the target cities were caused by combined effects of active photochemical reactions, horizontal transports and vertical transports of ozone from the upper layer. Note that the ozone at high altitudes was also formed by photochemical reactions.

Source apportionment of ozone

We quantified the contributions of different regions to ozone in eastern China with the WRF-CMAQ/ISAM source apportionment model. The spatial contributions of emission sources from various regions to the daytime ozone concentrations in eastern China are shown in Fig. 4a. Results show that local provincial-level emissions within a source region were the dominant contributor to surface ozone in Henan, Shandong, Jiangsu and Zhejiang provinces. Regional transports of ozone also significantly deteriorated the air quality in their surrounding areas. For example, emissions from Anhui increased the average daytime ozone in Jiangsu by 5–20 ppb, while the emissions from Hubei contributed up to 20 ppb to ozone concentrations in Henan, Shandong, Anhui and Jiangsu provinces. Influenced by the southwest wind, ozone from Shandong province increased the ozone concentrations in Bohai Sea by 25–75 ppb. However, the prevailing east and northeast winds at Bohai Sea transported air masses containing high ozone back to Beijing-Tianjin-Hebei and Shandong, considerably contributing to the persistence of high ozone concentrations in these regions (Fig. 2b). Boundary conditions were introduced into the ISAM model to account for the transport contribution of chemical species from areas outside the modeling domain. In our study, boundary conditions was an important contributor to the ambient ozone in the whole study region, particularly in Beijing-Tianjin-Hebei, Shanxi and Northern Shaanxi provinces. These super-regional transports from boundary conditions increased the surface ozone concentrations in eastern China by 5–60 ppb during the daytime on 6 June, 2021.

The diurnal variations in the contributions from regional sources to ozone in Zhengzhou, Suzhou, Xi'an and Dezhou are shown in Fig. 4b. Results show that the local province-level sources contributed more to ozone concentrations in the daytime than in other time, indicating the importance of local photochemical formation for the surface ozone increases. Compared with other sources, boundary condition contributions changed little with time and showed obvious spatial variations.

Table S1 shows the absolute and relative contributions of local source, regional transport and boundary conditions to the surface ozone concentrations averaged over daytime in the receptor cities. The contributions of regional transport were divided into inter-regional and outer-regional (OTH) transports based on the setting of the regional sources. For daytime average ozone, local sources contributed 51.9 ppb in Xi'an, 21.2 ppb in Linfen, 24.8 ppb in Hengshui, 52.2 ppb in Zhengzhou, 28.4 ppb in Dezhou, 20.7 ppb in Huainan, 33.2 ppb in Suzhou and 18.0 ppb in Taian to surface ozone concentrations. Local sources were the dominant contributors to ozone in Xi'an and Zhengzhou, accounting for 53.9% and 52.9% of the total ozone, respectively. Inter-regional transport was the primary contributor to daytime ozone in Dezhou with 34.2%, Suzhou with 42.6%, and Taian with 36.3%.

Outer-regional transport contributed less than 18% to daytime ozone in the receptor cities. The high contributions of boundary conditions to ozone increases in receptor cities during the transport processes, observed in this work, is comparable to the previous investigations (Kwok et al. 2015; Han et al. 2018; Pay et al. 2019; Shu et al. 2019). We found that boundary conditions were an important contributor to daytime ozone in Linfen with 52.9%, Hengshui with 44.5%, Huainan with 27.5%, and Taian with 35.5%. Shu et al. (2020) reported that under the weather condition of anticyclone, ozone in the Yangtze River Delta was dominated by local productions. While our study demonstrated that in addition to local productions, regional transports from the surrounding Zhejiang was also an important source of ozone in Jiangsu. Our source apportionment results showed that the combined effects of emissions from local provinces and regional

transports were responsible for the serious ozone pollution in eastern China.

Conclusion

In this study, the historical orange-alert large-scale ozone pollutiont episode on 6 June 2021 in eastern China was investigated on the basis of observations and simulations. During the episode, 93.7% (89 out of 95) of the cities in eastern China suffered ozone pollution, which was severe than ever reported. The prevailing northwest wind in the upper troposphere and the Western Pacific subtropical high at sea provided favorable meteorological conditions with high temperature and low relative humidity for the active photochemical formations of ozone, resulting in the rapid increases of ozone concentrations. Anticyclone in the low troposphere controlled the Yangtze River Delta region and contributed to the persistence of high ozone concentrations there. Regional transports of ozone from surrounding Henan, Shandong and the Bohai sea deteriorated the ozone pollution in Beijing-Tianjin-Hebei and led to the continuing high concentrations after sunset. During daytime, the situ formations of aloft ozone aggravated surface ozone pollution through vertical downward transports. The model source attribution results confirmed the important role of local provincial-level emissions and regional transports in the formation of this large-scale regional ozone pollution in eastern China. This study provided insights into drivers of the large-scale and persistent ozone pollution episode in eastern China on 6 June, 2021. Our results demonstrate that the locally and regionally coordinated emission control actions should be considered to alleviate severe regional ozone pollutions.

Supplementary Information The online version contains supplementary material available at https://doi.org/10.1007/s10311-022-01421-0.

Acknowledgements This work was partially supported by National Natural Science Foundation of China (No. 42175084, 21577126, and 41561144004), the Department of Science and Technology of China (No. 2018YFC0213506, 2018YFC0213503, and 2016YFC0202702) and National Research Program for Key Issues in Air Pollution Control in China (No. DQGG0107). Part of this work was also supported by the "Zhejiang 1000 Talent Plan" and Research Center for Air Pollution and Health in Zhejiang University. Pengfei Li is supported by National Natural Science Foundation of China (no. 22006030), Initiation Fund for Introducing Talents of Hebei Agricultural University (412201904), and Hebei Youth Top Q15 Fund (BJ2020032).

References

Bloomer BJ, Stehr JW, Piety CA et al (2009) Observed relationships of ozone air pollution with temperature and emissions. Geophys Res Lett 36:L09803. https://doi.org/10.1029/2009GL037308

Boer GJ (1993) Climate change and the regulation of the surface moisture and energy budgets. Clim Dyn 8:225–239. https://doi.org/10.1007/BF00198617

Chang KL, Petropavlovskikh I, Cooper OR et al (2017) Regional trend analysis of surface ozone observations from monitoring networks in eastern North America, Europe and East Asia. Elementa 5:1–22. https://doi.org/10.1525/elementa.243

Chen R, Riyu L (2016) Role of large-scale circulation and terrain in causing extreme heat in Western North China. J Climate. https://doi.org/10.1175/JCLI-D-15-0254.1

Cheng N, Chen Z, Sun F et al (2018) Ground ozone concentrations over Beijing from 2004 to 2015: Variation patterns, indicative precursors and effects of emission-reduction. Environ Pollut 237:262–274. https://doi.org/10.1016/j.envpol.2018.02.051

Finch DP, Palmer PI (2020) Increasing ambient surface ozone levels over the UK accompanied by fewer extreme events. Atmos Environ 237:117627. https://doi.org/10.1016/j.atmosenv.2020.117627

Gao J, Zhu B, Xiao H et al (2016) A case study of surface ozone source apportionment during a high concentration episode, under frequent shifting wind conditions over the Yangtze River Delta, China. Sci Total Environ 544:853–863. https://doi.org/10.1016/j.scitotenv.2015.12.039

Gao M, Gao J, Zhu B et al (2020) Ozone pollution over china and india: seasonality and sources. Atmos Chem Phys 20:4399–4414. https://doi.org/10.5194/acp-20-4399-2020

Gao D, Xie M, Liu J et al (2021) Ozone variability induced by synoptic weather patterns in warm seasons of 2014–2018 over the Yangtze River Delta region, China. Atmos Chem Phys 21:5847–5864. https://doi.org/10.5194/acp-21-5847-2021

Gong C, Liao H (2019) A typical weather pattern for ozone pollution events in North China. Atmos Chem Phys 19:13725–13740. https://doi.org/10.5194/acp-19-13725-2019

Gong C, Liao H, Zhang L et al (2020) Persistent ozone pollution episodes in North China exacerbated by regional transport. Environ Pollut 265:115056. https://doi.org/10.1016/j.envpol.2020.115056

Gu Y, Li K, Xu J et al (2020) Observed dependence of surface ozone on increasing temperature in Shanghai. China Atmos Environ 221:11708. https://doi.org/10.1016/j.atmosenv.2019.117108

Guo JJ, Fiore AM, Murray LT et al (2018) Average versus high surface ozone levels over the continental USA: Model bias, background influences, and interannual variability. Atmos Chem Phys 18:12123–12140. https://doi.org/10.5194/acp-18-12123-2018

Han X, Zhu L, Wang S et al (2018) Modeling study of impacts on surface ozone of regional transport and emissions reductions over North China Plain in summer 2015. Atmos Chem Phys 18:12207–12221. https://doi.org/10.5194/acp-18-12207-2018

Jacob DJ, Winner DA (2009) Effect of climate change on air quality. Atmos Environ 43:51–63. https://doi.org/10.1016/j.atmosenv.2008.09.051

Jaén C, Udina M, Bech J (2021) Analysis of two heat wave driven ozone episodes in Barcelona and surrounding region: Meteorological and photochemical modeling. Atmos Environ 246:118037. https://doi.org/10.1016/j.atmosenv.2020.118037

Jenkin ME (2008) Trends in ozone concentration distributions in the UK since 1990: Local, regional and global influences. Atmos Environ 42:5434–5445. https://doi.org/10.1016/j.atmosenv.2008.02.036

Jerrett M, Burnett RT, Pope CA et al (2009) Long-term ozone exposure and mortality. N Engl J Med 360:1085–1095. https://doi.org/10.1056/nejmoa0803894

Jin L, Tonse S, Cohan DS et al (2008) Sensitivity analysis of ozone formation and transport for a central California air pollution episode. Environ Sci Technol 42:3683–3689. https://doi.org/10.1021/es072069d

Kalabokas P, Hjorth J, Foret G et al (2017) An investigation on the origin of regional springtime ozone episodes in the western Mediterranean. Atmos Chem Phys 17:3905–3928. https://doi.org/10.5194/acp-17-3905-2017

Kwok RHF, Baker KR, Napelenok SL, Tonnesen GS (2015) Photochemical grid model implementation and application of VOC, NOx, and O_3 source apportionment. Geosci Model Dev 8:99–114. https://doi.org/10.5194/gmd-8-99-2015

Lelieveld J, Evans JS, Fnais M et al (2015) The contribution of outdoor air pollution sources to premature mortality on a global scale. Nature 525:367–371. https://doi.org/10.1038/nature15371

Li L, Chen C, Huang C et al (2012) Process analysis of regional ozone formation over the Yangtze River Delta, China using the Community Multi-scale Air Quality modeling system. Atmos Chem Phys 12:10971–10987. https://doi.org/10.5194/acp-12-10971-2012

Li G, Bei N, Cao J et al (2017) Widespread and persistent ozone pollution in eastern China during the non-winter season of 2015: Observations and source attributions. Atmos Chem Phys 17:2759–2774. https://doi.org/10.5194/acp-17-2759-2017

Li K, Jacob DJ, Liao H et al (2019) Anthropogenic drivers of 2013–2017 trends in summer surface ozone in China. Proc Natl Acad Sci U S A 116:422–427. https://doi.org/10.1073/pnas.1812168116

Li K, Jacob D, Shen L et al (2020) Increases in surface ozone pollution in China from 2013 to 2019: anthropogenic and meteorological influences. Atmos Chem Phys 20:11423–11433. https://doi.org/10.5194/acp-20-11423-2020

Li K, Jacob DJ, Liao H et al (2021) Ozone pollution in the North China Plain spreading into the late-winter haze season. Proc Natl Acad Sci U S A 118:e2015797118. https://doi.org/10.1073/pnas.2015797118

Liu J, Wang L, Li M et al (2019) Quantifying the impact of synoptic circulation patterns on ozone variability in northern China from April to October 2013–2017. Atmos Chem Phys 19:14477–14492. https://doi.org/10.5194/acp-19-14477-2019

Lu X, Hong J, Zhang L et al (2018) Severe surface ozone pollution in china: a global perspective. Environ Sci Technol Lett 5:487–494. https://doi.org/10.1021/acs.estlett.8b00366

Lu X, Zhang L, Wang X et al (2020) Rapid Increases in Warm-Season surface ozone and resulting health impact in China since 2013. Environ Sci Technol Lett 7:240–247. https://doi.org/10.1021/acs.estlett.0c00171

Malley CS, Henze DK, Kuylenstierna JCI et al (2017) Updated global estimates of respiratory mortality in adults ≥ 30 years of age attributable to long-term ozone exposure. Environ Health Perspect 125:0807021. https://doi.org/10.1289/EHP1390

Mao J, Wang L, Lu C et al (2020) Meteorological mechanism for a large-scale persistent severe ozone pollution event over eastern China in 2017. J Environ Sci (china) 92:187–199. https://doi.org/10.1016/j.jes.2020.02.019

MEP: China National Ambient Air Quality Standards, GB3095- 2012, MEP, Beijing, China, 2012.

Nie E, Zheng G, Gao D et al (2019) Emission characteristics of VOCs and potential ozone formation from a full-scale sewage sludge composting plant. Sci Total Environ 659:664–672. https://doi.org/10.1016/j.scitotenv.2018.12.404

Otero N, Sillmann J, Schnell JL et al (2016) Synoptic and meteorological drivers of extreme ozone concentrations over Europe. Environ Res Lett 11:024005. https://doi.org/10.1088/1748-9326/11/2/024005

Paoletti E, De MA, Beddows DCS et al (2014) Ozone levels in European and USA cities are increasing more than at rural sites, while peak values are decreasing. Environ Pollut 192:295–299. https://doi.org/10.1016/j.envpol.2014.04.040

Pay MT, Gangoiti G, Guevara M et al (2019) Ozone source apportionment during peak summer events over southwestern Europe. Atmos Chem Phys 19:5467–5494. https://doi.org/10.5194/acp-19-5467-2019

Pu X, Wang T, Huang X et al (2017) Enhanced surface ozone during the heat wave of 2013 in Yangtze River Delta region, China. Sci Total Environ 603–604:807–816. https://doi.org/10.1016/j.scitotenv.2017.03.056

Schnell JL, Prather MJ, Josse B et al (2016) Effect of climate change on surface ozone over North America, Europe, and East Asia. Geophys Res Lett 43:3509–3518. https://doi.org/10.1002/2016GL068060

Shu L, Xie M, Wang T et al (2016) Integrated studies of a regional ozone pollution synthetically affected by subtropical high and typhoon system in the Yangtze River Delta region, China. Atmos Chem Phys 16:15801–15819. https://doi.org/10.5194/acp-16-15801-2016

Shu L, Wang T, Xie M et al (2019) Episode study of fine particle and ozone during the CAPUM-YRD over Yangtze River Delta of China: characteristics and source attribution. Atmos Environ 203:87–101. https://doi.org/10.1016/j.atmosenv.2019.01.044

Shu L, Wang T, Han H et al (2020) Summertime ozone pollution in the Yangtze River Delta of eastern China during 2013–2017: Synoptic impacts and source. Environ Pollut 257:113631. https://doi.org/10.1016/j.envpol.2019.113631

Simon H, Reff A, Wells B et al (2015) Ozone trends across the United States over a period of decreasing NOx and VOC emissions. Environ Sci Technol 49:186–195. https://doi.org/10.1021/es504514z

Skarby L, Ro-Poulsen H, Wellburn FAM, Sheppard LJ (1998) Impacts of ozone on forests: a European perspective. New Phytol 139:109–122. https://doi.org/10.1046/j.1469-8137.1998.00184.x

Sun L, Xue L, Wang Y et al (2019) Impacts of meteorology and emissions on summertime surface ozone increases over central eastern China between 2003 and 2015. Atmos Chem Phys 19:1455–1469. https://doi.org/10.5194/acp-19-1455-2019

Tang G, Liu Y, Huang X et al (2021) Aggravated ozone pollution in the strong free convection boundary layer. Sci Total Environ 788:147740. https://doi.org/10.1016/j.scitotenv.2021.147740

Vellingiri K, Kim KH, Lim JM et al (2016) Identification of nitrogen dioxide and ozone source regions for an urban area in Korea using back trajectory analysis. Atmos Res 176–177:212–221. https://doi.org/10.1016/j.atmosres.2016.02.022

Verstraeten WW, Neu JL, Williams JE et al (2015) Rapid increases in tropospheric ozone production and export from China. Nat Geosci 8:690–695. https://doi.org/10.1038/ngeo2493

Wang T, Xue L, Brimblecombe P et al (2017) Ozone pollution in China: a review of concentrations, meteorological influences, chemical precursors, and effects. Sci Total Environ 575:1582–1596. https://doi.org/10.1016/j.scitotenv.2016.10.081

Wang L, Li M, Yu S et al (2020) Unexpected rise of ozone in urban and rural areas, and sulfur dioxide in rural areas during the coronavirus city lockdown in Hangzhou, China: implications for air quality. Environ Chem Lett 18:1713–1723. https://doi.org/10.1007/s10311-020-01028-3

Wang L, Chen X, Zhang Y, Huang Y (2021) Article Switching to electric vehicles can lead to significant Switching to electric vehicles can lead to significant reductions of $PM_{2.5}$ and NO_2 across China. One Earth 4:1037–1048. https://doi.org/10.1016/j.oneear.2021.06.008

Xia N, Du E, Guo Z, de Vries W (2021) The diurnal cycle of summer tropospheric ozone concentrations across Chinese cities: Spatial patterns and main drivers. Environ Pollut 286:117547. https://doi.org/10.1016/j.envpol.2021.117547

Xu J, Huang X, Wang N et al (2021) Understanding ozone pollution in the Yangtze River Delta of eastern China from the perspective of diurnal cycles. Sci Total Environ 752:141928. https://doi.org/10.1016/j.scitotenv.2020.141928

Xue L, Wang T, Gao J et al (2014) Ground-level ozone in four Chinese cities: precursors, regional transport and heterogeneous processes. Atmos Chem Phys Discuss 14:20767–20803. https://doi.org/10.5194/acpd-14-20767-2014

Xue T, Liu J, Zhang Q et al (2019) Rapid improvement of $PM_{2.5}$ pollution and associated health benefits in China during 2013–2017. Sci China Earth Sci 62:1847–1856. https://doi.org/10.1007/s11430-018-9348-2

Yang X, Wu K, Lu Y et al (2021) Origin of regional springtime ozone episodes in the Sichuan Basin, China: role of synoptic forcing and regional transport. Environ Pollut 278:116845. https://doi.org/10.1016/j.envpol.2021.116845

Yu SC, Eder B, Dennis R, Chu SH (2006) New unbiased symmetric metrics for evaluation of air quality models. Atmos Sci Lett 7:26–34. https://doi.org/10.1002/asl.125

Yu SC, Mathur R, Pleim J et al (2014) Aerosol indirect effect on the grid-scale clouds in the two-way coupled WRF-CMAQ: model description, development, evaluation and regional analysis. Atmos Chem Phys 14:11247–11285

Zhang R, Lei W, Tie X, Hess P (2004) Industrial emissions cause extreme urban ozone diurnal variability. Proc Natl Acad Sci U S A 101:6346–6350. https://doi.org/10.1073/pnas.0401484101

Zhang Q, Zheng Y, Tong D et al (2019) Drivers of improved $PM_{2.5}$ air quality in China from 2013 to 2017. Proc Natl Acad Sci U S A 116:24463–24469. https://doi.org/10.1073/pnas.1907956116

Zheng Y, Jiang F, Feng S et al (2021) Long-range transport of ozone across the eastern China seas: a case study in coastal cities in southeastern China. Sci Total Environ 768:144520. https://doi.org/10.1016/j.scitotenv.2020.14452

Supplementary Material

Model configuration

The physical parameterizations used in the Weather Research and Forecasting (WRF) model included the two-moment Morrison cloud microphysics scheme, the Rapid Radiative Transfer Model for General Circulation Models (RRTMG) longwave and shortwave radiation parameterizations, the Kain-Fritsch (KF2) cumulus cloud scheme, the Pleim-Xiu (PX) land-surface scheme and the asymmetric convective model (ACM2) for a planetary boundary layer (PBL) scheme (Pleim, 2007). Meteorological initial and lateral boundary conditions used in the WRF model were provided by the ERA-Interim reanalysis dataset archived at a spatial resolution of $1^0 \times 1^0$ and a temporal resolution of 6 h. The carbon bond gas-phase chemical mechanism (CB05) and aerosol chemistry scheme of AERO6 were used in the Community Multiscale Air Quality (CMAQ) modeling system. The anthropogenic emissions were taken from the Multi-resolution Emission Inventory for China version 1.2 (MEICv1.2) (http://www.meicmodel.org) for 2019. Biogenic emissions were estimated by the Biogenic Emissions Inventory System version 3.14 (BEISv3.14). The default initial (IC) and chemical boundary conditions (BCON) were used.

Model evaluation

The evaluations of model performances on O_3 and NO_2 concentrations in selected cities are presented in Table S1. As shown in Figs 1c, 1d and S3, the CMAQ model well reproduced the observed diurnal characteristics of O_3 concentrations. Generally, the model captured the diurnal variations of O_3 (NO_2) in selected cities in eastern China, with MB and NMB values ranging from -5.9 to 11.6 ppb (-1.3 to 2.9 ppb) and -6.6% to 19.5% (-3.6% to 16.3%), respectively. The model simulations showed very good correlations with observations with R values higher than 0.9 for both O_3 and NO_2 in the 8 selected cities.

Characteristics of O_3 pollution from June 7 to 10

From June 7 to 9, O_3 pollution was slightly alleviated compared with June 6, but the central and eastern China still suffered light and moderate O_3 pollution, respectively and some specific cities were exposed to severe pollution (Fig S2). By June 10, the air quality in the study area improved significantly. The O_3 pollution levels in Henan and Shandong, the most seriously polluted areas, changed from moderate to slight with the air quality in parts of the remaining areas showing good or excellent.

Synoptic meteorological conditions of the O_3 pollution

Fig S4 shows the composited synoptic weather conditions including geopotential heights at 500 hPa in East Asia, mean wind fields at 500 hPa, sea level pressure, maximum temperatures (T_{max}) and wind fields at 850 hPa, vertical velocity values at 500 hPa, 850 hPa and 1000 hPa in eastern China on 6 June, 2021. There were a low-pressure system over the Northeast China and a strong Western Pacific subtropical high at sea (Fig S4a). Located behind the East Asian trough, northwestern winds prevailed in upper air and brought dry and hot weather (Figs S4b, c). Finch and Palmer (2020) analyzed the temperature dependence of O_3 exceedances in the United Kingdom during 1999-2019, indicating that when the temperatures in the rural (urban) areas were higher than 18 ℃ (21 ℃), these areas suffered O_3 exceedances. At the junction of the Beijing-Tianjin-Hebei, Henan and Shandong provinces, there was a weak low-pressure and high temperature with T_{max} reaching over 40℃, which was in favor of the occurrence of O_3 pollution. The anticyclone at 850 hPa in the Yangtze River Delta region indicated that there were downward atmospheric motions, which were conductive to the accumulation of pollutants (Fig S4c). As shown in Figss S4d-f, the positive vertical velocity values at 500 hPa, 850 hPa and 1000 hPa in eastern China suggested that pollutants would be transported from high altitudes to lower troposphere and the ground, which have been identified as a typical feature of O_3 pollution (Gong et al. 2019; Shi et al. 2018; Mao et al. 2020). The deep atmospheric sinking motions characterized by positive high vertical velocities (>0.3 Pa s^{-1}) at 500 hPa in the Yangtze River Delta favored the accumulation of pollutants and may resulted in high O_3 concentrations on the

ground. At 850 hPa, the negative vertical velocities in the southern Beijing-Tianjin-Hebei indicated upward airflows. However, at 1000 hPa, the airflows in the southern Beijing-Tianjin-Hebei switched from rising to sinking, which may be caused by the urban-breeze circulations. Overall, the synoptic weather in eastern China on 6 June 2021 was conductive to the formation and accumulation of high O_3 concentrations and the occurrences of O_3 pollution on the ground.

Evolutions of O_3 pollution and corresponding meteorological conditions from 5 to 10 June

Fig S6a shows the spatial distributions of the meteorological fields at 15:00 when the O_3 concentrations were the highest in each day from 5 to 10 June, 2021. The northward movement of the West Pacific Subtropical High (WPSH) brought water vapor and increased the relative humidity along the way, leading to the decreases of O_3 concentrations in the Yangtze River Delta region. As shown in Figs S6b, and S6c, T2 in the junction of Beijing-Tianjin-Hebei, Henan and Anhui decreased and the relative humidity increased during 7-9 June, leading to the decreases of O_3 concentrations. At the same time, the O_3 concentrations in Shandong province increased from 7 to 8 June, mainly due to the enhancementd of local chemical formations under favorable meteorological conditions with decreases of relative humidity and continuous regional transports from Henan, Anhui and Jiangsu provinces. On 10 June, the O_3 pollution levels in Shandong province and the Yangtze River Delta region were significantly improved by the wet scavenging effects of precipitation on 9 June, 2021 (Fig S6d).

Process analysis of O_3 formation

The contribution of each process to O_3 formation in Linfen was similar to that in Xi'an, while the contribution of each process in Hengshui was similar to that in Dezhou (Fig S7a). For Taian, vertical transport (VTRA) was the principal contributor, with positive contribution values of 6.9-32.1 ppb h^{-1} throughout the day, indicating the important role of vertical transports in raising the O_3 levels in Taian. Gas-phase chemistry (CHEM) significantly contributed to daytime O_3 increases at both near-surface and aloft levels, with the average contributions of 1.5-11.2, 0.9-7.3, 0.6-7.4, 1.0-10.7 ppb h^{-1} for Linfen, Hengshui, Huainan and Taian, respectively (Fig S7b). The daytime mean contributions of vertical transport to the surface O_3 were 26.4, 8.1, and 17.0 ppb h^{-1} for Linfen, Huainan and Taian, respectively. Influenced by the updraft air, vertical transport showed minor effects on the O_3 formation in Dezhou (1.7 ppb h^{-1}), and even destructed the O_3 in Hengshui (-7.2 ppb h^{-1}). Horizontal transport played a positive role in the daytime O_3 formation in Hengshui (11.8 ppb h^{-1}) and Dezhou (4.1 ppb h^{-1}), due to the transports of O_3 containing air masses from the Bohai Sea and Henan province, as discussed in Section 3.2.

Although chemical ozone formation weakened after 16:00, ozone concentrations in the selected cities remained at a high level between 17:00 and 23:00. Therefore, we also explored the contributions of gas-phase chemistry, vertical transport, horizontal transport and dry deposition during nighttime (17:00-23:00) to ozone concentrations. Compared to the gas-phase chemistry and dry deposition, vertical and horizontal transports were main contributors to O_3 changes during nighttime. At night, horizontal transports imported O_3 into Xi'an, Dezhou, Linfen and Hengshui, with average positive contributions of 15.4, 27.5, 16.7 and 32.9 ppb h^{-1}, respectively, but the positive effects of VTRA on O_3 increases were partly offset by vertical transports with mean values of -15.7, -22.8, 9.0 and -28.0 ppb h^{-1}, respectively. For Zhengzhou, Suzhou, Huainan and Taian, vertical transports increased the surface concentrations of nighttime O_3 at rates of 9.4, 16.6, 3.8 and 14.6 ppb h^{-1}, respectively. Higher contribution values from the gas-phase chemistry were found in the urban areas, which were attributed to abundant O_3 precursor emissions and favorable meteorological conditions, including strong solar radiation, high temperature and low relative humidity (Figs 2b, 2c). Horizontal transports made higher contributions to coastal cities than those in the inland regions due to the sea-land breeze circulations. Vertical transports decreased the high O_3 concentrations in the coastal areas. For vertical transport, high contribution values were observed in southeast China due to the influence of the strong anticyclone (Fig 2c). Similar to the spatial distributions of vertical transport, dry deposition showed high negative contribution values in southeast China varying from -0.1 to -56.9 ppb h^{-1}.

References

Gong C, Liao H, Zhang L, et al (2020) Persistent ozone pollution episodes in North China exacerbated by regional transport. Environ Pollut 265:115056. https://doi.org/10.1016/j.envpol.2020.115056

Mao J, Wang L, Lu C, et al (2020) Meteorological mechanism for a large-scale persistent severe ozone pollution event over eastern China in 2017. J Environ Sci (China) 92:187–199. https://doi.org/10.1016/j.jes.2020.02.019

Pleim JE (2007) A combined local and nonlocal closure model for the atmospheric boundary layer. Part I: model description and testing. J Appl Meteorol Clim 46:1383–1395. https ://doi.org/10.1175/ JAM25 39.1

Shi C, Yuan R, Wu B, et al (2018) Meteorological conditions conducive to $PM_{2.5}$ pollution in winter 2016/2017 in the Western Yangtze River Delta, China. Sci Total Environ 642:1221–1232. https://doi.org/10.1016/j.scitotenv.2018.06.137

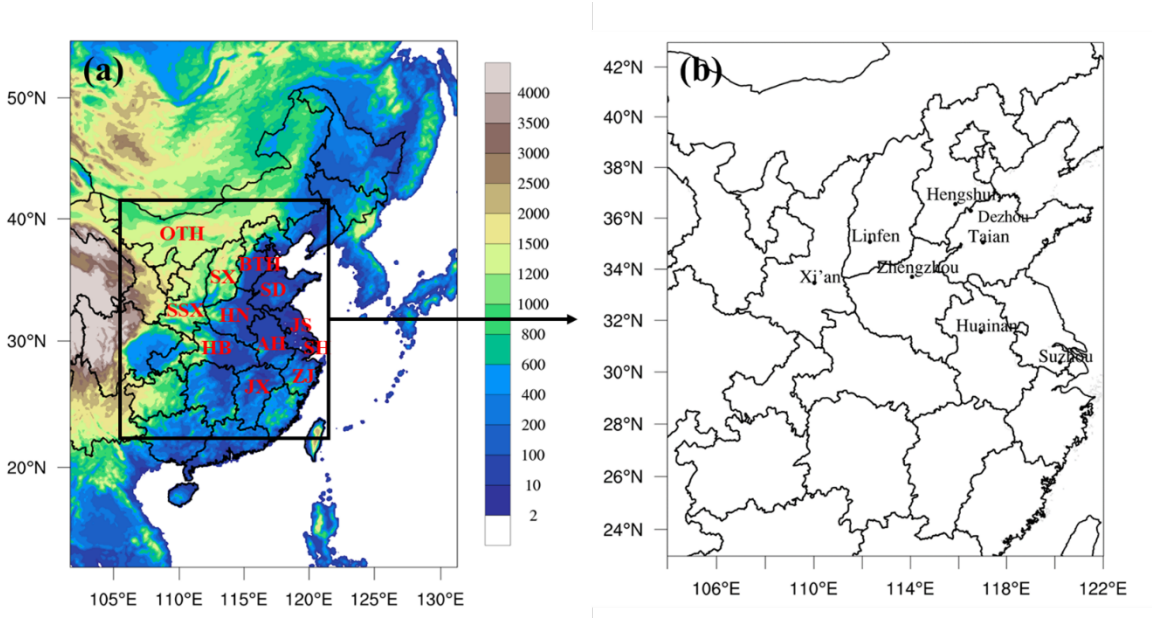

Figure S1. (a) Model simulation domain with terrain heights (m) for source apportionment of O_3; (b) The study area and locations of the eight selected key cities. The tracked source regions are shown in the figure: BTH: Beijing-Tianjin-Hebei; SX: Shanxi; SSX: Shaanxi; SD: Shandong; HN: Henan; HB: Hubei; AH: Anhui; JS: Jiangsu; SH: Shanghai; ZJ: Zhejiang; JX: Jiangxi; OTH: Other region except the marked areas in the simulation domain.

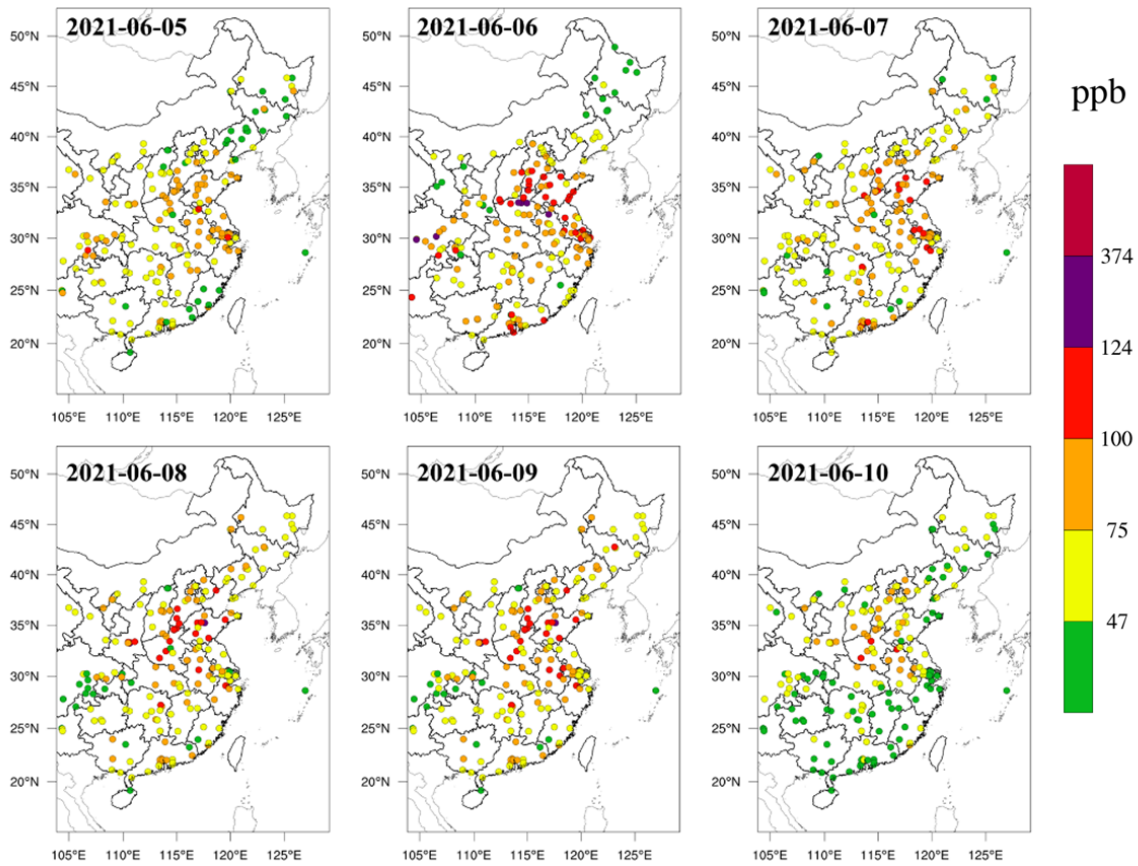

Figure S2. Spatial distributions of observed MDA8 (daily maximum 8-h average) O_3 concentrations in eastern China from 5 to 10 June, 2021.

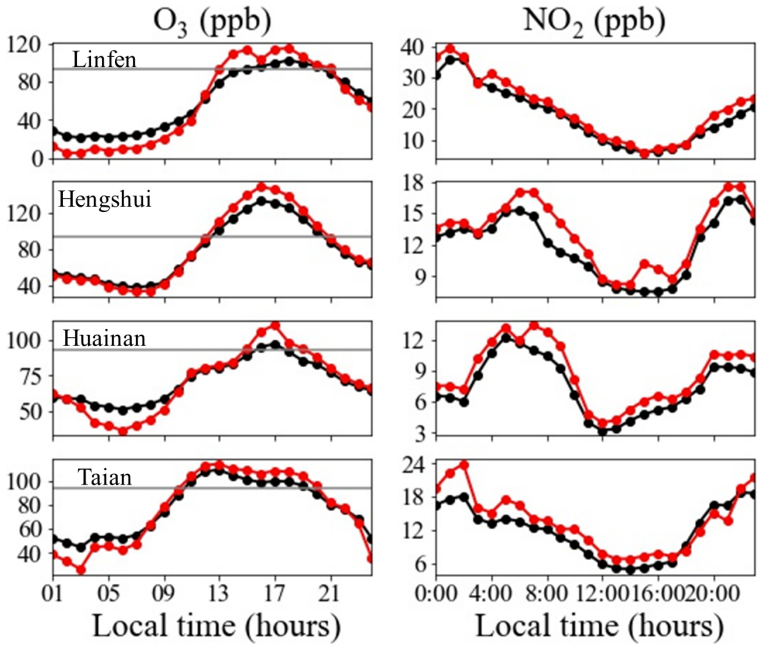

Figure S3. Diurnal variations of observed versus simulated O_3 concentrations (left column) and NO_2 concentrations (right column) in Linfen, Hengshui, Huainan and Taizhou on 6 June, 2021. The grey lines represent the grade II of national O_3 standard of 93.5 ppb.

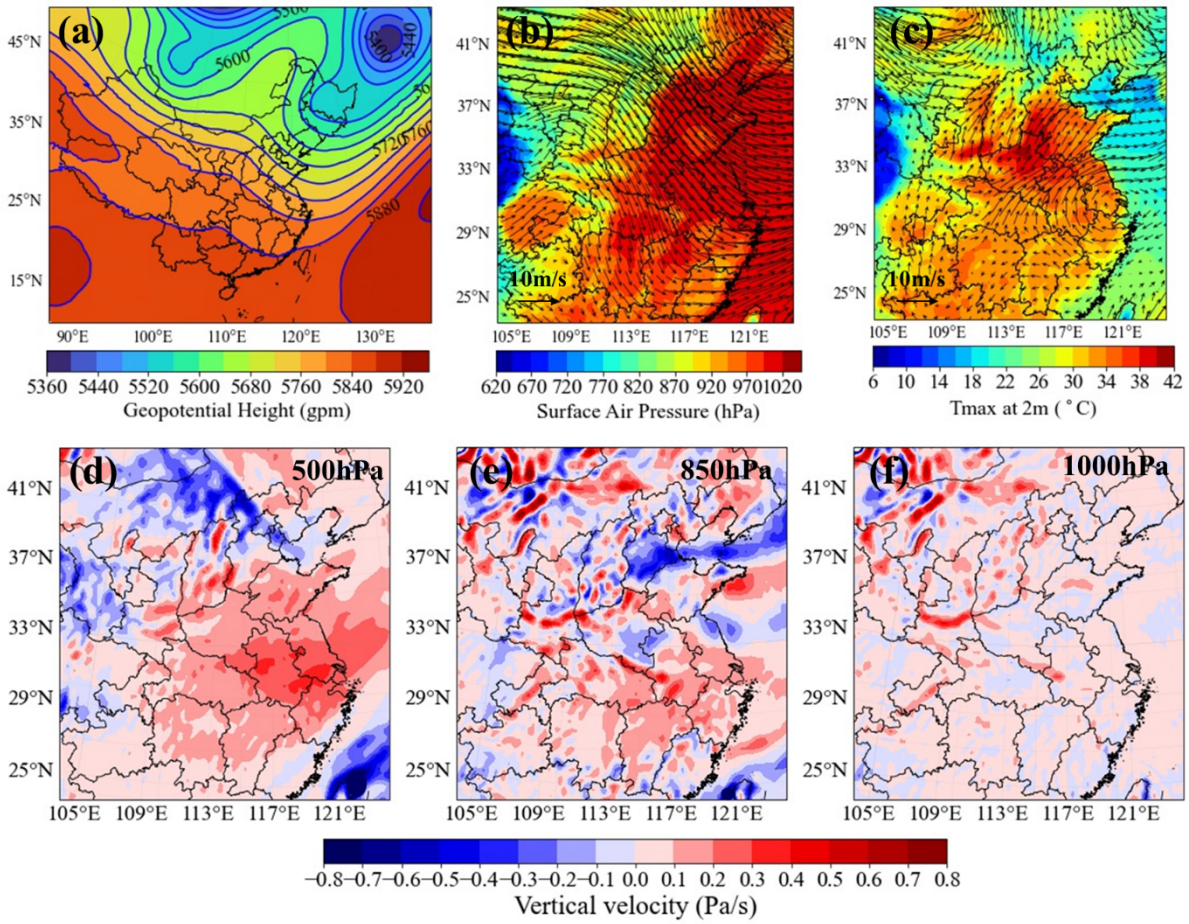

Figure S4. Composite distributions of (a) geopotential heights at 500 hPa; (b) daily mean wind fields at 500 hPa and surface air pressure (shade); (c) daily mean wind fields at 850 hPa and daily maximum temperatures at the surface (shade); (d) daily mean vertical velocity at 500 hPa; (e) daily mean vertical velocity at 850 hPa; and (f) daily mean vertical velocity at 1000 hPa on 6 June of 2021.

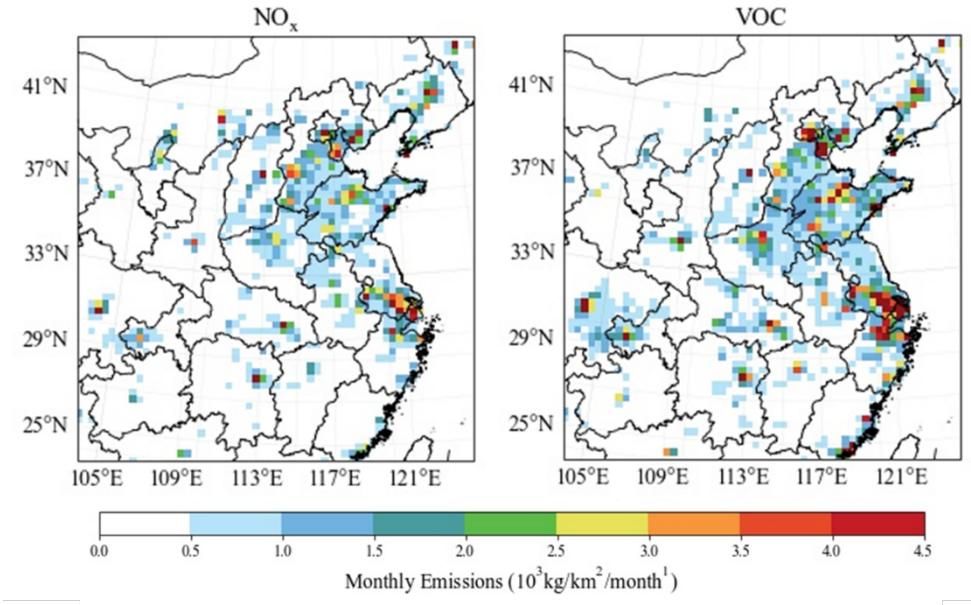

Figure S5. Monthly total emissions of NOx and VOCs (volatile organic compounds) for June, 2021.

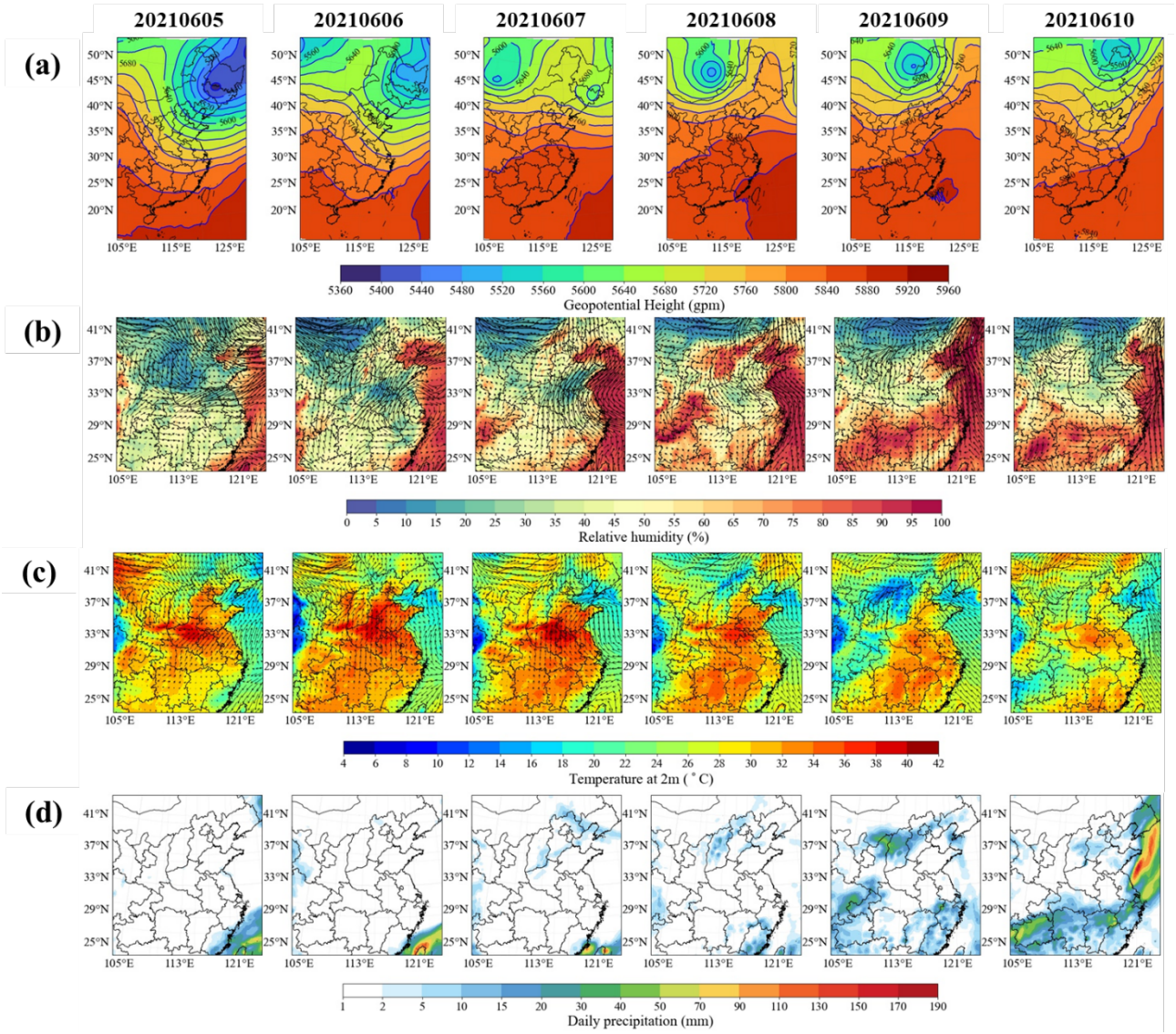

Figure S6. Composites of (a) geopotential heights at 500hPa, (b) daily mean 10 m wind fields and 2 m temperature fields (shaded colors); (c) daily mean surface relative humidity and wind fields at 850 hPa; (d) daily total precipitation from 5 to 10 June, 2021.

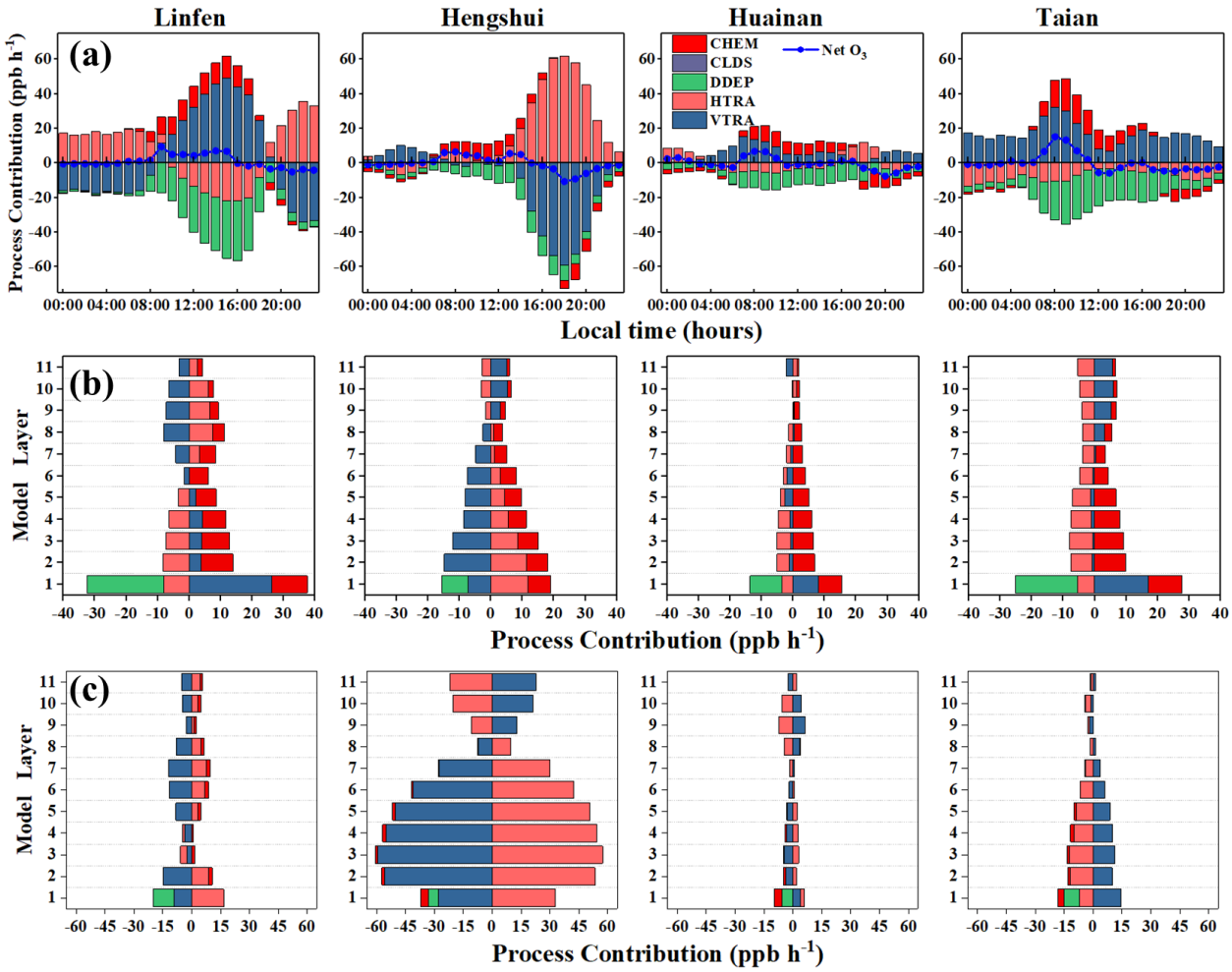

Figure S7. (a) Hourly contributions of different processes to O_3 formation with blue line presenting the net O_3 changes; (b) vertical profiles of daytime (8:00-16:00) and (c) nighttime (17:00-23:00) mean process contributions to O_3 changes at different heights in Linfen, Hengshui, Huainan and Taian on 6 June, 2021.

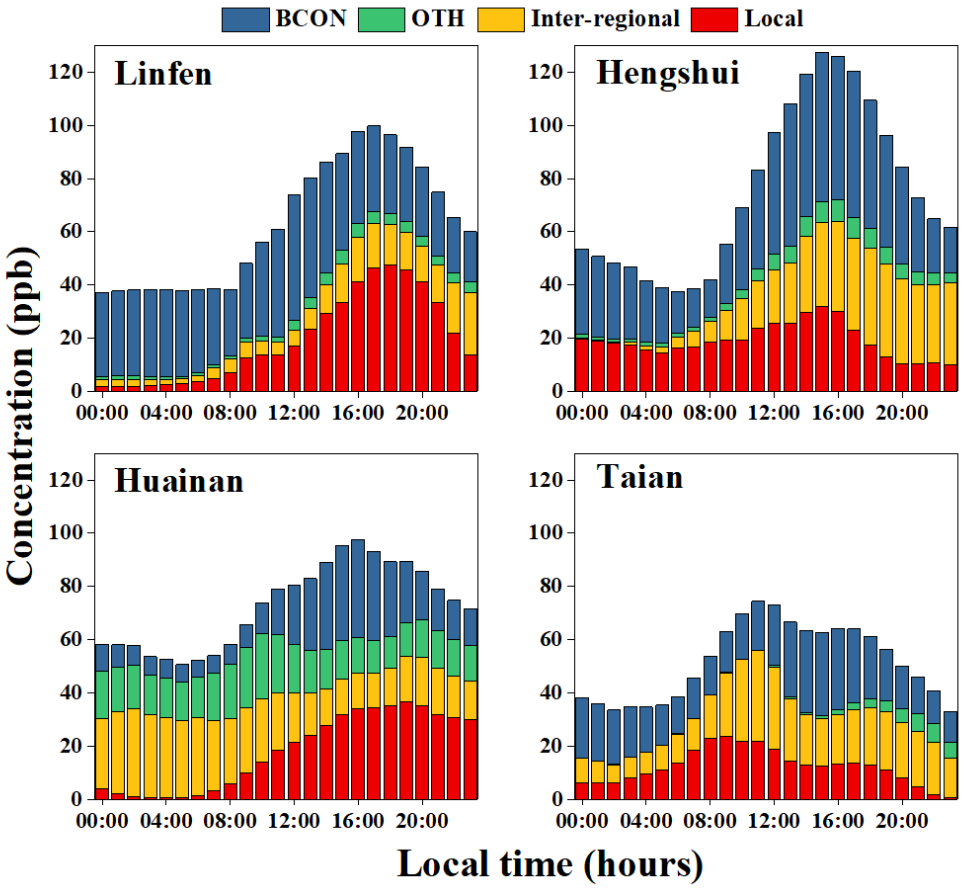

Figure S8. O_3 source apportionments of O_3 contributed by Local (local provincial), Inter-regional, OTH (other regions in the simulation domain) and BCON (boundary condition) source regions in Linfen, Hengshui, Huainan and Taian on 6 June, 2021.

Table S1. Comparison between model simulations and observations for O_3 and NO_2 in the 8 selected cities on 6 June, 2021.

		O_3 (ppb)	NO_2 (ppb)
Zhengzhou	OBS	87.1	13.8
	PRE	81.4	14.6
	MB	-5.8	0.8
	NMB	-6.6%	5.9%
	R	0.98	0.91
Suzhou	OBS	72.8	17.2
	PRE	73.8	19.0
	MB	1.0	1.9
	NMB	1.4%	10.9%
	R	0.98	0.97
Xi'an	OBS	59.7	24.6
	PRE	71.3	27.5
	MB	11.6	2.9
	NMB	19.5%	11.7%
	R	0.97	0.95
Dezhou	OBS	84.7	10.5
	PRE	82.7	10.1
	MB	-2.0	-0.4
	NMB	-2.4%	-3.6%
	R	0.98	0.93
Linfen	OBS	56.9	17.9
	PRE	59.5	19.9
	MB	2.6	2.0
	NMB	4.5%	11.3%
	R	0.98	0.98
Hengshui	OBS	80.9	11.9
	PRE	77.5	13.2
	MB	-3.5	1.3
	NMB	-4.3%	10.9%
	R	0.99	0.96
Huainan	OBS	70.6	7.5
	PRE	71.1	8.7
	MB	0.5	1.2
	NMB	0.7%	16.3%
	R	0.97	0.97
Taian	OBS	77.0	11.9
	PRE	77.9	13.6
	MB	0.9	1.7
	NMB	1.2%	14.4%
	R	0.99	0.93

OBS observed average value of monitoring sites, *PRE* simulated concentration, *MB* mean bias, *NMB* normalized mean bias, *R* correlation coefficient

Table S2. Average contributions of source regions to daytime (8:00-16:00) O_3 in the 8 receptor cities on 6 June of 2021.

	Local	Inter-regional	OTH	BCON	Local	Inter-regional	OTH	BCON
	Absolute contribution (ppb)				Relative contribution (%)			
Zhengzhou	52.2	15.4	4.8	26.2	52.9	15.6	4.9	26.5
Suzhou	33.2	40.1	8.1	12.8	35.2	42.6	8.6	13.6
Xi'an	52.0	0.0	20.7	23.8	53.9	0.0	21.4	24.7
Dezhou	28.4	33.4	7.4	28.5	29.1	34.2	7.5	29.2
Linfen	21.2	8.6	3.2	37.1	30.3	12.2	4.6	52.9
Hengshui	24.8	21.1	5.2	40.9	26.9	22.9	5.7	44.5
Huainan	20.7	18.9	18.5	22.1	25.8	23.6	23.1	27.5
Taian	20.0	23.8	0.6	23.3	27.4	36.3	0.1	36.2